Concrete-filled bimetallic tubes under axial compression: Experimental investigation

Yong Ye [a], Lin-Hai Han [b,*], Therese Sheehan [c], Zi-Xiong Guo [a]

[a] *College of Civil Engineering, Huaqiao University, Xiamen, 361021, P. R. China*

[b] *Department of Civil Engineering, Tsinghua University, Beijing, 100084, P. R. China*

(Corresponding author, E-mail address: lhhan@tsinghua.edu.cn)

[c] *School of Engineering, University of Bradford, Bradford, BD7 1DP, United Kingdom*

Abstract: This paper presents the experimental results of axial compression tests on concrete-filled bimetallic tubes (CFBT). The cross section of the bimetallic tube is composed of an outer layer made of stainless steel and an inner layer made of carbon steel. A total of 12 specimens with a circular cross section were tested under axial compression. The test parameters included the thickness of the stainless steel tube layer (t_{ss}=0-1.36 mm) and the compressive strength of the infilled concrete (f_{cu}=21.1-42.8 MPa). Test results showed that, the two layers of the bimetallic tube worked well together, and the CFBT specimens exhibited ductile characteristics. The influence of the parameters on the failure mode, load versus deformation relationship, axial compressive strength, and strain development of the tested specimens were investigated. Finally, the feasibility of three existing design codes for predicting the axial compressive strength of CFST under axial compression was evaluated.

Keywords: Concrete-filled bimetallic tubes (CFBT); Axial compression; Composite action; Stainless steel; Experimental investigation

Nomenclature

A_c	Cross sectional area of core concrete
A_s	Cross sectional area of steel tube
A_{sc}	Cross sectional area of carbon steel tube layer
A_{ss}	Cross sectional area of stainless steel tube layer
D	Outer diameter of column
E_c	Elastic modulus of concrete
E_s	Elastic modulus of steel
f_{ck}	Characteristic compressive strength of concrete
f_{cu}	Cube compressive strength of concrete
f_c'	Cylinder compressive strength of concrete
f_y	Yield strength of steel
f_{yc}	Yield strength of carbon steel
L	Specimen length
N	Axial load
N_u	Axial compressive strength
p	Contact stress
SI	Strength index
t_{sc}	Wall thickness of carbon steel tube layer
t_{ss}	Wall thickness of stainless steel tube layer
t_t	Total wall thickness of steel tube
Δ	Axial deformation
Δ_u	Axial deformation corresponding to peak load
$\bar{\varepsilon}$	Mean longitudinal strain
ε_l	Longitudinal strain
ε_s	Strain of steel
ε_t	Transverse strain
ε_{yc}	Yield strain of carbon steel
ξ	Confinement factor
$\sigma_{0.2s}$	0.2% proof stress of stainless steel

1. Introduction

Concrete-filled steel tubular (CFST) structures have been applied in practical engineering more and more widely in the last decades, especially in high-rise, or even super high-rise buildings, and long-span bridges [1]. The successful application of CFST structures is due to its mechanical and constructional advantages such as high strength and easy installation. So far, a great number of investigations have been carried out on the structural behavior of CFST members [2-8].

Carbon steel is still the most common material that used in the steel tube of a CFST member. When exposed to humidity and air, carbon steel always suffers from corrosion due to its natural characteristics. In order to deal with the problem of corrosion, additional measures, such as painting or plating, are necessary to insure the durability of the carbon steel tube. On the other hand, the use of stainless steel in structural engineering has attracted an accelerating interest around the world [9]. Stainless steel is known to be extremely durable, corrosion resistant, and easily maintained. One of the promising methods to fully utilize the mechanical behavior of stainless steel in structures is to use hollow sections filled with concrete, otherwise known as concrete filled stainless steel tubes (CFSST). The mechanical behaviour of CFSST members has also been studied by some researchers [10-12]. However, compared with mild carbon steel, the structural use of stainless steel is still in its infancy, mainly inhibited by the high cost. The cost of stainless steel is still several times that of mild carbon steel, so more efforts should be made to make better use of the stainless steel at this stage.

Nowadays, there is a growing demand for innovative materials with properties that are not achievable with individual conventional ones in different fields, and "hybrid materials" have attracted much attention from the researchers [13]. In particular, bimetallic materials can provide favorable combinations of structural and functional properties. As an example, stainless steel-clad

carbon steel tubes show several advantages, such as increased corrosion resistance as compared to all-carbon steel tubes and reduced cost as compared to all-stainless steel tubes. The bimetallic tubes have been used as handrails in municipal engineering, as shown in Fig. 1.

With the purpose of further utilizing the advantages of stainless steel and compensating for its high cost, an innovative concrete filled bimetallic tube (CFBT) is proposed in this paper. Fig. 2(b) shows a schematic of the CFBT, which is composed of a bimetallic tube and the concrete core. The cross section of the bimetallic tube comprises an outer layer made of stainless steel and an inner layer made of carbon steel. It is expected that a CFBT column will ideally combine the advantages of both stainless steel and conventional concrete filled steel tubes. On the other hand, the stainless steel possesses an obvious strain hardening beahviour and large elongation at breakage, the mechanical performance of the stainless steel tube layer in a CFBT column should be considered from an economic point of view.

To the authors' knowledge, there has been no research on this type of composite section. Before this type of composite members can be adopted in the structural engineering, extensive research on CFBT members should be conducted. The purpose of the experimental investigation conducted in this paper is threefold: (1) to provide initial test data pertaining to the axial compressive behaviour of CFBT short columns; (2) to study the difference in mechanical behaviour between CFBT and CFST columns; and (3) to study the influence of different parameters on the compressive strength of CFBT members.

2. Experimental program

2.1 General description

An experimental program involving ten CFBT and two reference CFST column specimens with circular cross sections were fabricated and tested under axial compression. Fig. 2 shows the

schematic view of cross sections of the CFST and CFBT specimens, where D is the overall diameter of the cross section; t_{ss} is the wall thickness of the stainless steel tube layer in the CFBT column. For CFST specimens, t_{sc} is the wall thickness of the steel tube, while for CFBT specimens, t_{sc} is the wall thickness of the carbon steel tube layer. The diameter of the CFST specimens was 165 mm. The CFBT specimens in the current tests were manufactured by capping an additional stainless steel plate to the flank surface of the CFST columns, so the diameter of the CFBT specimens was (165+2t_{ss}) mm, where t_{ss} was in millimeters. The length (L) of all of the column specimens was set as 615 mm. The experimental parameters included:

- Thickness of the stainless steel tube layer (t_{ss}=0.52 mm, 0.80 mm, or 1.36 mm);
- Cube compressive strength of the concrete (f_{cu}=21.1 MPa, 30.2 MPa, or 42.8 MPa).

A summary of the test information is presented in Table 1, where t_t is the total wall thickness of the tube; t_t equals to t_{sc} and t_{sc}+t_{ss} for CFST and CFBT specimens, respectively. The specimen labels in Table 1 are designated according to the following rules: (1) "CFST-_" and "t_c_-_" stand for the CFST and CFBT specimens respectively; (2) for CFBT specimens, the character "t" stands for the thickness of the stainless steel tube layer, and "c" represents the compressive strength of the infilled concrete; (3) the last number after the hyphen stands for the different specimen in the same test group. Two identical samples were prepared and tested under each condition to confirm the reliability of the experimental results.

For conventional CFST members, a confinement factor (ξ) is often used to assess the confinement effect of concrete core provided by the outer steel tube [15]. The definition of ξ is as follows:

$$\xi = \frac{A_s f_y}{A_c f_{ck}} \tag{1}$$

where A_s and A_c are the cross sectional areas of steel tube and concrete core, respectively; f_y is the yield stress of steel; and f_{ck} is the characteristic compressive strength of concrete.

In order to evaluate the confinement effect in CFBT members, a similar confinement factor (ξ) is defined based on the expected composite action between the two steel tube layers, as follows:

$$\xi = \frac{A_{sc} f_{yc} + A_{ss} \sigma_{0.2s}}{A_c f_{ck}} \tag{2}$$

Where A_{sc} and A_{ss} are the cross sectional areas of carbon steel tube layer and stainless steel tube layer, respectively; f_{yc} is the yield strength of the carbon steel; and $\sigma_{0.2s}$ is the 0.2% proof stress of the stainless steel.

2.2 Specimen preparation and material properties

The bimetallic tubes used to fabricate the CFBT columns were manufactured on the basis of carbon steel tubes, which were identical to those used in the CFST columns. The carbon steel tube was manufactured by rolling a flat plate into a cylindrical shell and then welding the seam at room temperature. The bimetallic tube was made by rolling a flat stainless steel plate round the above carbon steel tube and welding the longitudinal seam using full-penetration groove weld. Before manufacturing the bimetallic tube, the outer surface of the carbon steel tube was properly treated and the rust was removed. The rolling process of the stainless steel plate was carefully conducted to ensure the interfacial contact and reduce the possible gap between the stainless steel tube layer and the carbon steel tube layer. For a bimetallic tube, the weld seam in the stainless steel tube layer was staggered from that in the carbon steel tube layer. The two tube layers were fully welded together at both ends to prevent air and water from leaking into the layer-layer gap and inducing corrosion in the carbon steel. In practice, the bimetallic tube can be fabricated using different techniques and processes, with various combinations of the two tube layers to meet the specific application

requirement [14]. By adopting the currently available manufacturing technique, the sizes of the outer stainless steel tube layers could be satisfactorily matching those of the carbon steel tube layers.

Before casting the infilled concrete, a steel endplate was fixed temporarily to the tube at one end with tack welding. The concrete was poured into the tube layer by layer and fully vibrated to ensure the compactness. After the concrete had cured for two weeks, the top loose layer of mortar in the specimen was removed with a chisel and hammer. A layer of high-strength cement mortar was cast to the top of each column to ensure the flushness of the top surface. The endplate was then removed after the concrete had cured for four weeks.

Type 321 austenitic stainless steel according to ASTM A959-09 [16] was adopted to fabricate the bimetallic tubes. A series of coupon tests were carried out to determine the material properties of the stainless steel. The material test results showed that the stainless steel exhibited obvious nonlinear stress-strain responses, as shown in Fig.3. The main material test results of stainless steel are given in Table 2. The wall thickness of the carbon steel tube was 2.37 mm. The yield strength, ultimate strength, elastic modulus, and Poisson's ratio of the carbon steel were 287.5 MPa, 448.4 MPa, 207.4 GPa, and 0.294, respectively. For comparison purposes, the full-range stress-strain curve of the carbon steel is also presented in Fig. 3.

Three different concrete mixtures were designed with 28-day cube compressive strengths (f_{cu}) of approximately 20 MPa, 30 MPa, and 40 MPa. The mixtures were made with Portland cement, water, river sand, granitic stone of particle size 10-15 mm. The mix proportions and material properties of the concrete are shown in Table 3.

2.3 Test setup and instrumentation

A 5000 kN capacity hydraulic jack was used for the loading tests of all specimens. Fig. 4

shows a schematic view and photo of the test setup. The specimen was placed at the middle of the testing machine and the load was applied directly on the bottom of the specimen. Two steel clamps with a height of 60 mm were fixed at both ends of the column to ensure no local failure occur near the loading surfaces. Each steel clamp consisted of two semicircular parts and four high-strength bolts and nuts. The clearance between the clamps was 495 mm, approximately three times the outer diameter of all specimens.

For the CFST specimens, four strain gauges were adhered to the outer surface of the carbon steel tube to measure the strains on the mid-height section. For the CFBT specimens, four strain gauges were adhered to the inner surface of the carbon steel tube layer at mid-height and another four were set on the outer surface of the stainless steel tube layer at the same positions. The strain gauges were arranged perpendicular to or along the longitudinal direction of the specimen, as shown in Fig. 4(a). Four displacement transducers were arranged evenly at the four corners of the specimen to measure the axial shortening. All of the strain gauges and displacement transducers were connected to the data acquisition system and the readings were collected automatically every three seconds throughout the whole loading process. The unloading phase of each specimen was also recorded. A load interval of less than 1/10 of the estimated load-carrying capacity of the specimen was applied. The loading was terminated when one of the following circumstances occurred: (1) axial load dropped below 70% of its peak value; (2) weld failure in the steel tube occurred; or (3) nominal axial average strain of the specimen ($\bar{\varepsilon} = \Delta/L$, Δ is the axial shortening of the specimen) reached about 40,000 με, which corresponds to $\Delta \approx 25$ mm.

3. Experimental results and discussion

This section describes the primary experimental results of the test specimens, including the failure mode, axial load versus deformation relationship, ultimate strength, strain development of

the steel tube. The different axial behaviour between CFST and CFBT columns are also compared and discussed.

3.1 Failure modes

All of the CFST and CFBT column specimens failed in a ductile manner. The failure mode for both CFST and CFBT columns was a local (outward buckling) failure mechanism, as shown in Fig. 5. Compared with the conventional carbon steel CFST column [Fig. 5(a)], more local buckling appeared in the bimetallic tube of the CFBT columns although the final axial shortening for CFST and CFBT specimens was close. This is mainly attributed to the fact that the stainless steel material shows higher ductility and strain-hardening properties than the carbon steel. Once the bimetallic tube buckles, the stainless steel tube layer can provide effective hoop confinement to the inner carbon steel tube layer and enable the load to increase before new local buckling occurs at another position. Besides local buckling in the tube, weld fracture was also observed in the stainless steel tube layer for CFBT specimens t1c2-1 and t1c2-2 [Fig. 5(b)], probably due to the thinness of the stainless steel tube layer (t_{ss}=0.52 mm), which meant that the welding quality could not be fully guaranteed. Fig. 6 shows the weld seam at the location where the tube bulges. It should be noted that the weld fracture in specimen t1c2-1 had a different feature compared to that in specimen t1c2-2, as shown Fig. 6(a) and Fig. 5(b). The weld fracture was localized near the local buckle for specimen t1c2-1 [Fig. 6(a)], while the stainless steel tube layer was torn apart from the weld seam for specimen t1c2-2 [Fig. 5(b)]. For the other CFBT specimens, no weld fracture was observed during loading, see Fig. 6(b). To avoid fracture failure of the stainless steel tube layer, a minimum wall thickness of 0.80 mm is recommended when the stainless steel tube layer is manufactured following the process presented in this paper. If Fig. 5(a) and 5(f) is studied carefully, it can be found that inclined local buckles were observed in the tube of specimens CFST-1, CFST-2, t2c3-1

and t2c3-2, indicating that possible shear failure might have occurred in the concrete core.

After the loading test, the outer tube of the column specimen was removed to observe the failure mode of the concrete core. Furthermore, the stainless steel tube layer and carbon steel tube layer of the bimetallic tube were separated. Fig. 7 shows exposed views of the concrete core and different tube layers. It can be seen that the stainless steel tube layer and carbon steel tube layer generally buckled at the same positions, indicating the two tube layers can work well together. Meanwhile, local buckling could only occur in the stainless steel tube layer, as shown in Fig. 8. By adopting the technique in the current research to fabricate bimetallic tubes, there is almost no interfacial bond, resulting in incompatible buckling of the two tube layers. Nevertheless, the incompatibility was localized and the two tube layers generally deformed and buckled in coordination in the current research. In the future, it might be necessary to investigate the influence of bond between the two tube layers on the behaviour of CFBT members.

It can also be seen from Fig. 7 that, for both CFST and CFBT columns, the infilled concrete was crushed at the sections where local buckling in the tube occurred. As expected, an obvious shear plane in the concrete core was found to exist between the two main bulges of specimens CFST-2 and t2c3-1, as shown in Fig. 7(a) and 7(f). The shear-friction action on the interface contributed to the resistance of concrete core to the applied axial load.

Based on the above test observations, the typical failure modes of the CFBT columns can be classified into two types, i.e. Type A and Type B, as illustrated in Fig. 9(a) and 9(b). When ξ=0.678, the CFBT columns exhibited an obvious shear crack in the concrete core, accompanied by inclined bulges in the bimetallic tube [Fig. 9(a)]. When $\xi \geq 0.883$, local buckling occurred in the bimetallic tube and the concrete core was crushed [Fig. 9(b)]. Similar typical failure modes are found in CFST columns subjected to axial compression. According to the finding by Han (2007), when ξ is below

1.12, the CFST column tends to fail in the Type A failure mode [Fig. 9(a)]; as ξ increases beyond 1.12, the shear failure of concrete core is restrained by an increased confinement from the outer tube, and the CFST column fails in the Type B failure mode [Fig. 9(b)]. Compared to the carbon steel tube in a CFST column, the bimetallic tube in a CFBT column with the same confinement factor (ξ) can provide more confinement to concrete core, due to the higher strain-hardening capacity of the stainless steel material.

3.2 Axial load versus deformation relationships

The axial load (N) versus deformation (Δ) relationships for all specimens are presented in Fig. 10. The deformation is taken as the mean value of readings from four displacement transducers. It can be seen from Fig. 10 that, all the N-Δ curves for CFST and CFBT specimens exhibit ductile characteristics. The N-Δ curves for CFBT specimen t1c2-2 shows a descending branch after the peak point, which is different from that for the identical specimen t1c2-1. This is due to the wide-range weld fracture in the stainless steel tube layer in specimen t1c2-2. On the other hand, it seems that the localized weld fracture in the stainless steel tube layer [Fig. 6(a)] has no significant effect on the N-Δ response of specimen t1c2-1.

Generally, the N-Δ curves obtained from the tests can be classified into three types, which might depend on the magnitude of confinement factor (ξ). Fig. 11 shows the typical axial load (N) versus average strain (ε) curves for the CFBT columns, where $\varepsilon=\Delta/L$. The N-ε curve shifts from Type A to Type B and then to Type C as the confinement factor (ξ) increases. The corresponding curve types for all specimens are given in Table 1. Type A is the typical N-ε relationship with a strain-softening behaviour which is common for conventional CFST columns using carbon steel tubes. In the current research, the Type A N-ε curves were observed in CFST specimens CFST-1 and CFST-2 (ξ=0.723) and CFBT specimens t1c2-1 (ξ=0.883), t2c3-1 and t2c3-2 (ξ=0.678), owing to

the lower degree of tube confinement provided to the concrete, either caused by a relatively small tube thickness (t1c2-1) or high concrete strength (t2c3-1 and t2c3-2). For a Type A curve, the load decreases with an increase of axial deformation after the peak load (Point 1) and reaches Point 2. After that, the load increases once again to Point 3 at the end of the test, due to the strain hardening effect of both the carbon steel and stainless steel. Based on the test results, the corresponding load at Point 3 is generally larger than that at Point 1.

Compared with Type A, Type B N-ε curves exhibit similar characteristics except for the stable branch 1'2'. For a Type B curve, the load remains almost steady after reaching the peak value (Point 1'). Then the load increases once again to Point 3' when the test is terminated. The strain-hardening like response is also attributed to further stress development of the two steel materials. In the current research, the Type B N-ε curves were observed in CFBT specimens t2c2-1 and t2c2-2 (ξ=0.961), t3c2-1 and t3c2-2 (ξ=1.131), and t2c1-1 (ξ=1.376).

Type C is the typical N-ε relationship with a strain-hardening response. The CFBT specimen t2c1-2 (ξ=1.376) has an N-ε curve that can be classified as Type C. This type of curve has an initial linear-elastic branch followed by a transitional and linear-plastic branch. After the load reaches Point 1", there is a branch with a gradually decreasing slope until reaching Point 2". The nonlinear behaviour at this stage is due to the local buckling of the steel tube accompanied by the nonlinear response of the infilled concrete. After that, the N-ε curve increases almost linearly with a slope much smaller than that of the O1" branch, and the load reaches a peak value at the end of the test (Point 3"). This is probably attributed to the strain hardening of both the carbon steel and stainless steel materials. Since the stainless steel shows a much higher strain-hardening capacity than the carbon steel, the stainless steel layer of the bimetallic tube can exert effective confinement on the carbon steel layer and concrete core after experiencing substantial plastic deformation.

It is worthy to note that CFBT specimens t2c1-1 and t2c1-2 have a Type B and Type C N-ε curve, respectively, though their geometric dimensions and material properties are set as the same. The reason for this observation may be due to the fact that a possible gap can exist between the stainless steel tube layer and carbon steel tube layer. The gap postpones the interactions between the two tube layers and reduces the overall performance of the CFBT member. It is known that, the carbon steel tube layer dilates faster than stainless steel tube layer when the carbon steel tube layer buckles, and the carbon steel tube layer can get in contact with the stainless steel tube layer if the dimension of interfacial gap is within a certain limit. In the future, the influence of the possible gap between the stainless steel tube layer and carbon steel tube layer on the behaviour of CFBT members should be investigated if the bimetallic tube is fabricated following the technique described in this paper.

3.3 Load-carrying capacity

3.3.1 Axial compressive strength

For the specimens with a Type A or Type B N-ε curve, the axial compressive strength (N_u) is determined as the load corresponding to Point 1 or 1' in Fig. 11. While for the CFBT specimens having a Type C N-ε curve, the load keeps growing throughout the whole loading process, it is inappropriate to define Point 3" (Fig. 11) as the ultimate state since obvious local buckling has already occurred in the bimetallic tube. In these cases, N_u is determined corresponding to an axial strain (ε) of 10,000 με, at which the composite columns have experienced a sufficient deformation. The axial compressive strength (N_u) for all the CFST and CFBT specimens is listed in Table 1, where Δ_u is the axial deformation corresponding to N_u; and the asterisk indicates that Δ_u is corresponding to an axial strain of 10,000 με.

The influence of thickness of the stainless steel tube layer (t_{ss}) on the axial compressive

strength (N_u) of CFBT columns is shown in Fig. 12(a), where N_u is taken as the mean value of the two identical specimens for each test group. Within the range of test parameters herein (t_{ss}=0-1.36 mm), N_u increases almost linearly with the increase of t_{ss}. For a CFBT column subjected to axial compression, the confinement provided by the bimetallic tube renders the concrete core in a triaxial state of stress, in return, the bimetallic tube is supported by the concrete core from inside and becomes less sensitive to local buckling. A larger value of t_{ss} enables the stainless steel tube layer to carry more external loads, and at the same time provide more effective confinement to concrete core. The composite actions between the bimetallic tube and concrete core lead to increased axial compressive strength of the CFBT columns. In practice, the combination of the two tube layers in a bimetallic tube should be designed to meet the specific requirement of application, in-depth research on the optimized thickness ratio of stainless steel to carbon steel tube layers should be conducted.

The influence of concrete strength (f_{cu}) on the axial compressive strength (N_u) of CFBT columns is shown in Fig. 12(b), where N_u is also taken as the mean value of the two identical specimens for each test group. Within the test parameters in this research (f_{cu}=21.1-42.8 MPa), N_u tends to increase as f_{cu} increases.

3.3.2 Strength index

To evaluate the section capacity of the column specimens, a strength index (*SI*) is defined as follows:

$$SI = \frac{N_u}{A_{sc} f_{sc} + A_{ss}\sigma_{0.2s} + A_c f_c'} \tag{3}$$

where f_c' is the cylinder compressive strength of concrete and given by $f_c'=0.79f_{cu}$.

The strength indexes (*SI*) for all the specimens are listed in Table 1. The values of *SI* range

between 1.199 and 1.475, indicating effective composite actions between the steel tube and concrete core in enhancing the load-carrying capacity of the columns, as shown in Fig. 13, where p_1 is the contact stress between the concrete core and carbon steel tube layer, and p_2 is the contact stress between the carbon steel tube layer and stainless steel tube layer. Fig. 14 shows the relationship between *SI* and the confinement factor (ξ). It is obvious that, within the range of test parameters (ξ=0.678-1.376), *SI* tends to increase with increase of ξ. This is attributed to the fact that the concrete core can develop a higher uniaxial compressive strength under the lateral confinement of steel tube, and a stronger confinement leads to a higher strength enhancement of the concrete strength [15].

3.4 Strain analysis

The axial load (N) versus steel strain (ε_s) relationships of CFST and CFBT column specimens in each test group are shown in Fig. 15, where $\varepsilon_{l,carbon}$ and $\varepsilon_{t,carbon}$ denote the longitudinal and transverse strains of the carbon steel tube in CFST specimens and carbon steel tube layer in CFBT specimens; $\varepsilon_{l,stainless}$ and $\varepsilon_{t,stainless}$ denote the longitudinal and transverse strains of the stainless steel tube layer in CFBT specimens, respectively. The values of compressive strains are set as negative and the tensile ones positive in Fig. 15. It can be seen that, both the longitudinal and transverse strains of the carbon steel tube in CFST specimens and carbon steel tube layer in CFBT specimens attain the yield strain (ε_{yc} = 2121 με) before the axial compressive strength (N_u) is attained, which indicates that the strength of the carbon steel has been fully utilised. Besides, the strain development of the stainless steel tube layer generally agrees well with that of the carbon steel tube layer for the CFBT specimens. The above observation demonstrates that the stainless steel tube layer can work well with the carbon steel tube layer, and this behaviour is of vital significance for the CFBT section to fully develop its load-carrying capacity. Local buckling occurred near the position where strain

gauges were set for specimen t3c2-1, resulting in the differences of the strain readings between the two tube layers, as shown in Fig. 15(d).

4. Comparison with available design formula

So far, there have been some models to predict the ultimate strength of CFST and CFSST members. The CFSST models are often derived from those for CFST by replacing the terms related to carbon steel tubes with terms related to stainless steel tubes, like the yield stress of carbon steel is often replaced by 0.2% proof stress of stainless steel [4]. Since CFBT is actually a special form of CFST, it would be valuable to check whether the available models for CFST members are suitable for CFBT members. In this section, a comparison of the axial strength of CFBT columns obtained from experimental tests and predicted by ACI-318 (2002), Eurocode 4 (2004), and DBJ/T13-51-2010 (2010) codes is provided. During the calculation of the strength according to the above codes, the material partial safety factors are neglected and all the items related to the steel tube are replaced with those related to the bimetallic tube.

4.1 Description of the codes

4.1.1 ACI-318

The equation in ACI-318 [17] ignores the composite actions between the steel tube and concrete core, and considers the ultimate axial strength ($N_{u,ACI}$) of a CFST column as the summation of the individual strength of the steel tube and concrete core. The equation suggested by ACI-318 for circular CFST columns is given as:

$$N_{u,ACI} = A_s f_y + 0.85 A_c f_c' \tag{4}$$

While using Eq. (4) to calculate the strength of CFBT columns, $A_s f_y$ was replaced with $A_{sc} f_{sc} + A_{ss} \sigma_{0.2s}$.

4.1.2 Eurocode 4

The equation in Eurocode 4 (EC4) [18] takes into account the confinement effect of the core concrete provided by the outer steel tube. The EC4 equation for the axial strength ($N_{u,EC4}$) of a CFST is given as:

$$N_{u,EC4} = \eta_a A_s f_y + A_c f_c' \left(1 + \eta_c \frac{t}{D} \frac{f_y}{f_c'}\right) \quad (5)$$

where η_a=0.25(3+2 $\bar{\lambda}$)≤1.0, η_c=4.9-18.5 $\bar{\lambda}$ +17 $\bar{\lambda}^2$≥0, $\bar{\lambda}$ =($N_{pl,Rk}/N_{cr}$)$^{0.5}$, $N_{pl,Rk}$ can be calculated using Eq. (4) and the coefficient 0.85 is replaced by 1.0, $N_{cr}=\pi^2(EI)_{eff}/L^2$, $(EI)_{eff}=E_sI_s+0.6E_cI_c$; $\bar{\lambda}$ is the relative slenderness; $N_{pl,Rk}$ is the characteristic value of the plastic resistance to compression; N_{cr} is the elastic critical normal force for the relevant buckling mode; I_s and I_c are the second moments of area of the steel tube section and concrete section, respectively.

When Eq. (5) was used to calculate the strength of CFBT columns, A_sf_y was replaced by $A_{sc}f_{sc}+A_{ss}\sigma_{0.2s}$, t was replaced by $t_{ss}+t_{sc}$, and f_y in parenthesis was replaced by ($A_{sc}f_{yc}+A_{ss}\sigma_{0.2s}$)/($A_{sc}+A_{ss}$), $(EI)_{eff}=E_{sc}I_{sc}+E_{ss}I_{ss}+0.6E_cI_c$; I_{sc} and I_{ss} are the second moments of area of the carbon steel tube layer section and stainless steel tube layer section.

4.1.3 DBJ/T13-51-2010

The DBJ/T13-51-2010 [19] code also considers the enhancement of concrete strength due to the confinement effect by the outer tube. Following the DBJ/T13-51-2010 code, the axial strength ($N_{u,DBJ}$) of circular CFST columns is given as:

$$N_{u,DBJ} = f_{sc}A_t \quad (6)$$

where $f_{sc}=(1.14+1.02\xi)f_{ck}$; A_t is the total cross sectional area of the CFST column.

When Eq. (6) was used to calculate the strength of CFBT columns, the confinement factor (ξ) was obtained following Eq. (2), and $A_t=A_{ss}+A_{sc}+A_c$.

4.2 Verification and discussion

The feasibility of adopting the above design models to predict the axial compressive strength (N_u) of CFBT columns was examined herein. A comparison between the predicted strengths (N_{uc}) and experimental ones (N_{ue}) is given in terms of N_{uc}/N_{ue} versus confinement factor (ξ) relationship and shown in Fig. 16. It can be noted that, the above mentioned three codes generally underestimate the axial compressive strength of CFBT columns. The ACI-318 code gives the most conservative predictions as expected, since it does not consider the strength enhancement of concrete core induced by the confinement from the steel tube in a CFBT column. The mean value of $N_{u,ACI}/N_{ue}$ is 0.713 with a coefficient of variation of 0.0581. The DBJ/T13-51-2010 code also gives conservative predictions, and the mean value of $N_{u,DBJ}/N_{ue}$ is 0.829 with a coefficient of variation of 0.0632. Compared with the ACI-318 code and DBJ/T13-51-2010 code, EC4 yields the best predictions. The mean value of $N_{u,EC4}/N_{ue}$ is 0.935 with a coefficient of variation of 0.0419. It can be seen that, although the DBJ/T13-51-2010 and ACI-318 codes consider the confinement effect of the core concrete offered by the outer steel tube, the predictions are still conservative for CFBT columns, mainly due to the different material properties between the stainless steel and carbon steel. On the other hand, it is interesting to note that, all the three codes provide a more and more conservative prediction as the confinement factor (ξ) increases within the parameter range (ξ=0.678-1.376). This is probably due to the fact that the stainless steel shows much higher strain-hardening capacity than the carbon steel, and as the amount of stainless steel increases in a CFBT column, the strength enhancement of the concrete core is more obvious than that in a conventional CFST column. As a result, the current design codes could not be adopted directly to predict the axial compressive strength of CFBT columns. In order to improve the predictions, further research is needed, especially on the strength of concrete core under the confinement of bimetallic tube and on the bearing capacity of stainless steel tube layer when the ultimate state is reached.

5. Conclusions

This work presents an initial experimental investigation on the axial compressive behaviour of CFBT columns. Within the range of test parameters in this paper, the following conclusions can be drawn based on the above results:

(1) The CFBT columns behaved in a ductile manner. The failure mode of CFBT columns is the outward local buckling of the bimetallic tube and the crush of infilled concrete. Shear failure of infilled concrete was also observed for the CFBT specimen with a confinement factor (ξ) of 0.678.

(2) The strain development reveals that the outer stainless steel tube layer can work well together with the inner carbon steel tube layer. The two layers of the bimetallic tube generally buckle at the same positions at failure of CFBT columns.

(3) The axial load (N) versus deformation (Δ) relationships for CFBT columns can be classified into three typical types, and the shape of N-Δ curve is probably related to the confinement factor (ξ). The strain hardening behaviour of N-Δ curves is enhanced as ξ increases.

(4) With fixing the other parameters, the axial compressive strength of a CFBT column almost increases linearly with the increase of thickness of the stainless steel tube layer or the concrete strength.

(5) The ACI-318, DBJ/T13-51-2010, and EC4 codes give conservative predictions of the axial compressive strengths of CFBT columns, though the ACI-318 and DBJ/T13-51-2010 codes take into account the enhancement of concrete strength due to the confinement effect by the outer tube. Besides, the error increases as the confinement factor (ξ) increases.

Acknowledgements

The research reported in the paper is part of the Tsinghua University Initiative Scientific Research

Program (NO. 2013Z02) and the China Postdoctoral Science Foundation (No. 2015M571044). The support is greatly appreciated.

References

[1] L.H. Han, W. Li, R. Bjorhovde, Developments and advanced applications of concrete-filled steel tubular (CFST) structures: members, J. Constr. Steel Res. 100 (2014) 211-228.

[2] X.L. Zhao, L.W. Tong, X.Y. Wang, CFDST stub columns subjected to large deformation axial loading, Eng. Struct. 32(3) (2010) 692-703.

[3] B. Young, E. Ellobody, Experimental investigation of concrete-filled cold-formed high strength stainless steel tube columns, J. Constr. Steel Res. 62(5) (2006) 484-492.

[4] D. Lam, L. Gardner, Structural design of stainless steel concrete filled columns, J. Constr. Steel Res. 64(11) (2008) 1275-1282.

[5] J.Y.R. Liew, D.X. Xiong, Effect of preload on the axial capacity of concrete-filled composite columns, J. Constr. Steel Res. 65(3) (2009) 709-722.

[6] T. Perea, R. Leon, J. Hajjar, M. Denavit, Full-scale tests of slender concrete-filled tubes: Interaction behavior, J. Struct. Eng.-ASCE 140(9) (2014) 04014054.

[7] T. Sheehan, X.H. Dai, T.M. Chan, D. Lam, Structural response of concrete-filled elliptical steel hollow sections under eccentric compression, Eng. Struct. 45 (2012) 314-323.

[8] L.H. Han, Y. Ye, F.Y. Liao, Effect of core concrete initial imperfection on performance of eccentrically loaded CFST columns, J. Struct. Eng.-ASCE 142 (2016) 04016132.

[9] L. Gardner, The use of stainless steel in structures, Prog. Struct. Eng. Mat. 7(2) (2005) 45-55.

[10] M.F. Hassanein, O.F. Kharoob, Q.Q. Liang, Behaviour of circular concrete-filled lean duplex stainless steel tubular short columns, Thin-Walled Struct. 68 (2013) 113-123.

[11] M.F. Hassanein, O.F. Kharoob, Q.Q Liang, Behaviour of circular concrete-filled lean duplex stainless steel-carbon steel tubular short columns, Eng. Struct. 56 (2013) 83-94.

[12] B. Uy, Z. Tao, L.H. Han, Behaviour of short and slender concrete-filled stainless steel tubular columns, J. Constr. Steel Res. 67 (2011) 360-378.

[13] M.F. Ashby, Y.J.M. Bréchet, Designing hybrid materials, Acta Mater. 51(19) (2003) 5801-5821.

[14] Z. Fan, H. Yu, C. Li, Plastic deformation behavior of bi-metal tubes during magnetic pulse cladding: FE analysis and experiments, J. Mater. Process. Tech. 229 (2016) 230-243.

[15] L.H. Han, Concrete-filled steel tubular structures-theory and practice (2nd version), Beijing: China Science Press, 2007. [in Chinese]

[16] ASTM A959-09, Standard guide for specifying harmonized standard grade compositions for wrought stainless steels, West Conshohocken (PA): ASTM International, 2009.

[17] ACI-318, Building code requirements for reinforced concrete, Detroit (MI): American Concrete Institute, 2002.

[18] Eurocode 4, Design of composite steel and concrete structures, Part 1-1: general rules and rules for building, Brussels: EN 1994-1-1:2004, European Committee for Standardization, 2004.

[19] DBJ/T13-51-2010, Technical specifications for concrete-filled steel tubular structures (revised version), Fuzhou: Housing and Urban-Rural Development Department of Fujian Province, 2010. [in Chinese].

Tables

Table 1 Summary of test information

No.	Specimen label	t_{sc} (mm)	t_{ss} (mm)	t_t (mm)	D (mm)	$\sigma_{0.2s}$ (MPa)	f_{cu} (MPa)	ξ	Δ_u (mm)	N_u (kN)	SI	N-Δ curve type
1	CFST-1	2.37	Null	2.37	165.00	Null	30.2	0.723	2.67	1008	1.216	A
2	CFST-2	2.37	Null	2.37	165.00	Null	30.2	0.723	2.24	996	1.201	A
3	t1c2-1	2.37	0.52	2.89	166.04	283.3	30.2	0.883	4.83	1118	1.234	A
4	t1c2-2	2.37	0.52	2.89	166.04	283.3	30.2	0.883	5.11	1128	1.245	-
5	t2c2-1	2.37	0.80	3.17	166.60	274.6	30.2	0.961	6.15*	1215	1.288	B
6	t2c2-2	2.37	0.80	3.17	166.60	274.6	30.2	0.961	6.15*	1238	1.313	B
7	t3c2-1	2.37	1.36	3.73	167.72	275.8	30.2	1.131	6.15*	1345	1.312	B
8	t3c2-2	2.37	1.36	3.73	167.72	275.8	30.2	1.131	6.15*	1315	1.283	B
9	t2c1-1	2.37	0.80	3.17	166.60	274.6	21.1	1.376	6.15*	1151	1.442	B
10	t2c1-2	2.37	0.80	3.17	166.60	274.6	21.1	1.376	6.15*	1177	1.475	C
11	t2c3-1	2.37	0.80	3.17	166.60	274.6	42.8	0.678	3.28	1372	1.199	A
12	t2c3-2	2.37	0.80	3.17	166.60	274.6	42.8	0.678	3.50	1390	1.215	A

Table 2 Properties of the stainless steel

No.	Thickness (mm)	0.2% proof stress (MPa)	Ultimate strength (MPa)	Initial elastic modulus (GPa)	Poisson's ratio	Elongation at break
t1	0.52	283.3	811.6	194.8	0.296	0.529
t2	0.80	274.6	785.9	195.2	0.305	0.549
t3	1.36	275.8	765.3	199.7	0.299	0.541

Table 3 Mix proportions and material properties of the concrete

No.	Cement (kg/m^3)	Water (kg/m^3)	Sand (kg/m^3)	Coarse aggregate (kg/m^3)	Cube compressive strength (MPa)	Elastic modulus (GPa)
c1	335	195	650	1250	21.1	26.3
c2	410	195	620	1200	30.2	31.2
c3	420	168	320	1303	42.8	32.8

Figures

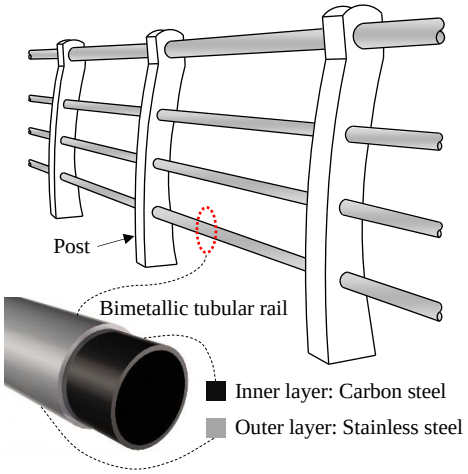

Fig. 1 Application of bimetallic tubes in handrails

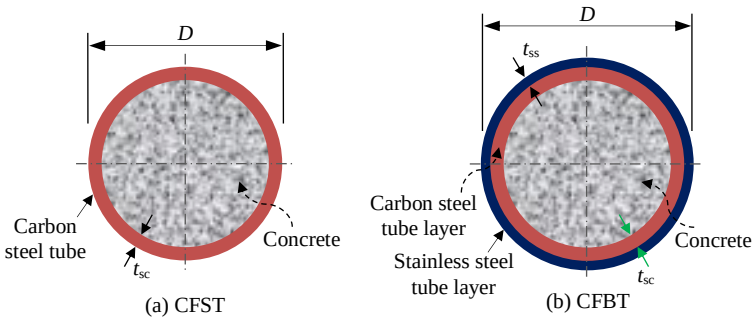

Fig. 2 Cross sections of circular CFST and CFBT columns

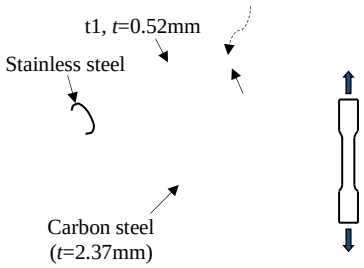

Fig. 3 Full-range stress-strain relationships of the carbon steel and stainless steel

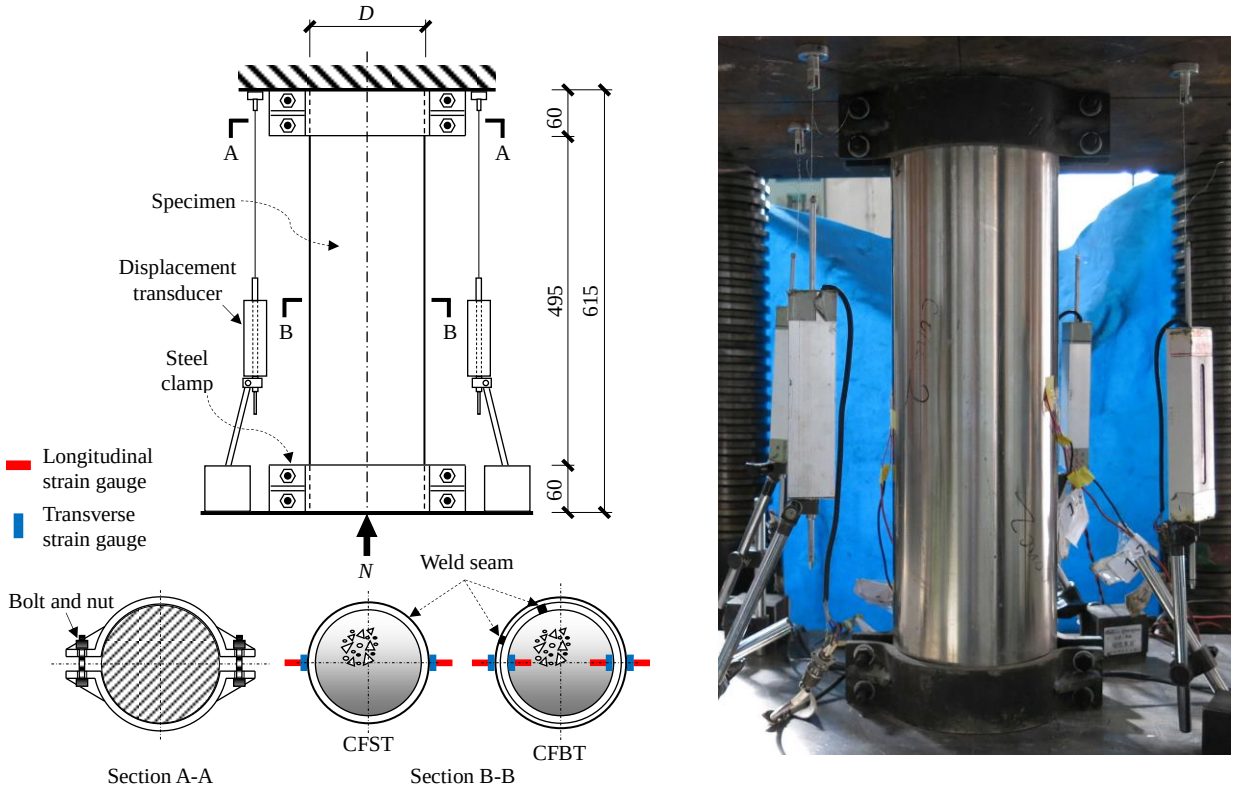

(a) Schematic view

(b) Test photo

Fig. 4 Schematic view and photo of the test specimen (unit: mm)

(a1) CFST-1 (a2) CFST-2 (b1) t1c2-1 (b2) t1c2-2 (c1) t2c2-1 (c2) t2c2-2

(d1) t3c2-1 (d2) t3c2-2 (e1) t2c1-1 (e2) t2c1-2 (f1) t2c3-1 (f2) t2c3-2

Fig. 5 Overall failure modes of the CFST and CFBT specimens

(a) t1c2-1 (t_o=0.5 mm) (b) t2c2-2 (t_o=0.80 mm)

Fig. 6 Local fracture of weld seam

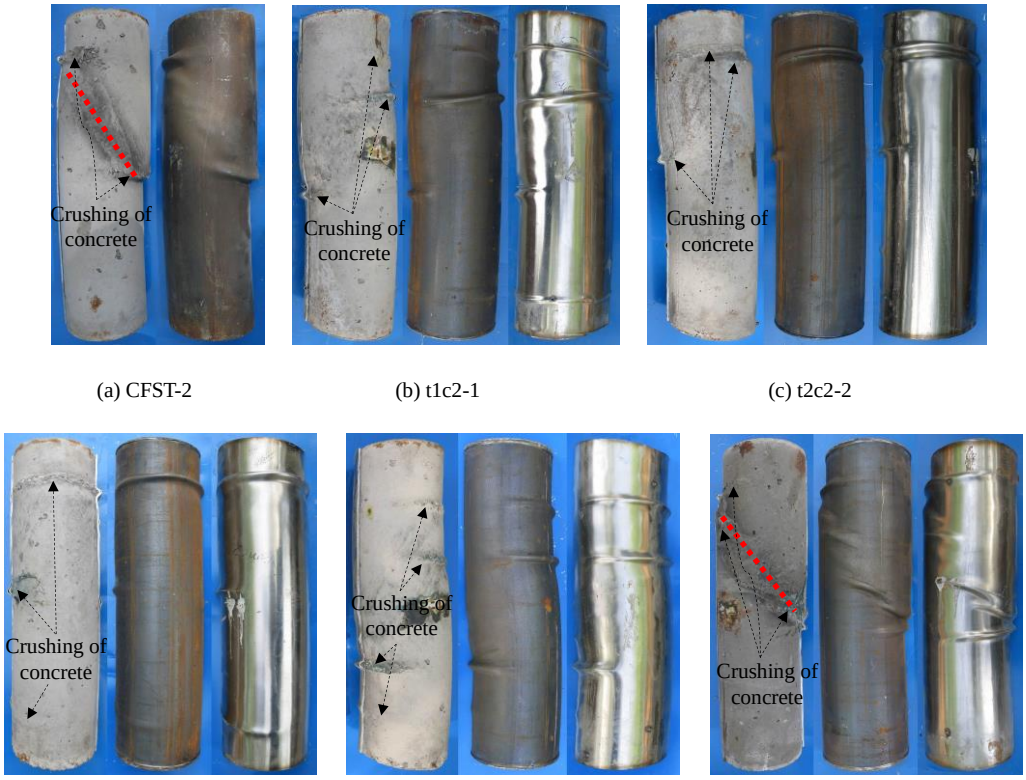

(a) CFST-2 (b) t1c2-1 (c) t2c2-2

(d) t3c2-2 (e) t2c1-1 (f) t2c3-1

Fig. 7 Failure appearances of different components of the specimens

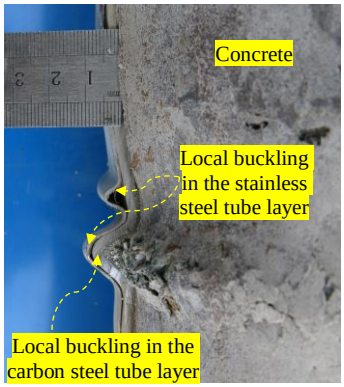

Fig. 8 Failure buckling features of the specimen t1c2-1

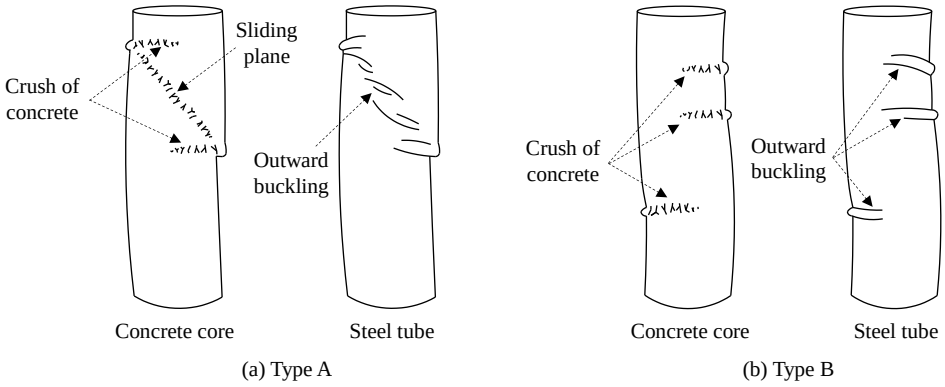

Fig. 9 Typical failure modes of CFBT short columns

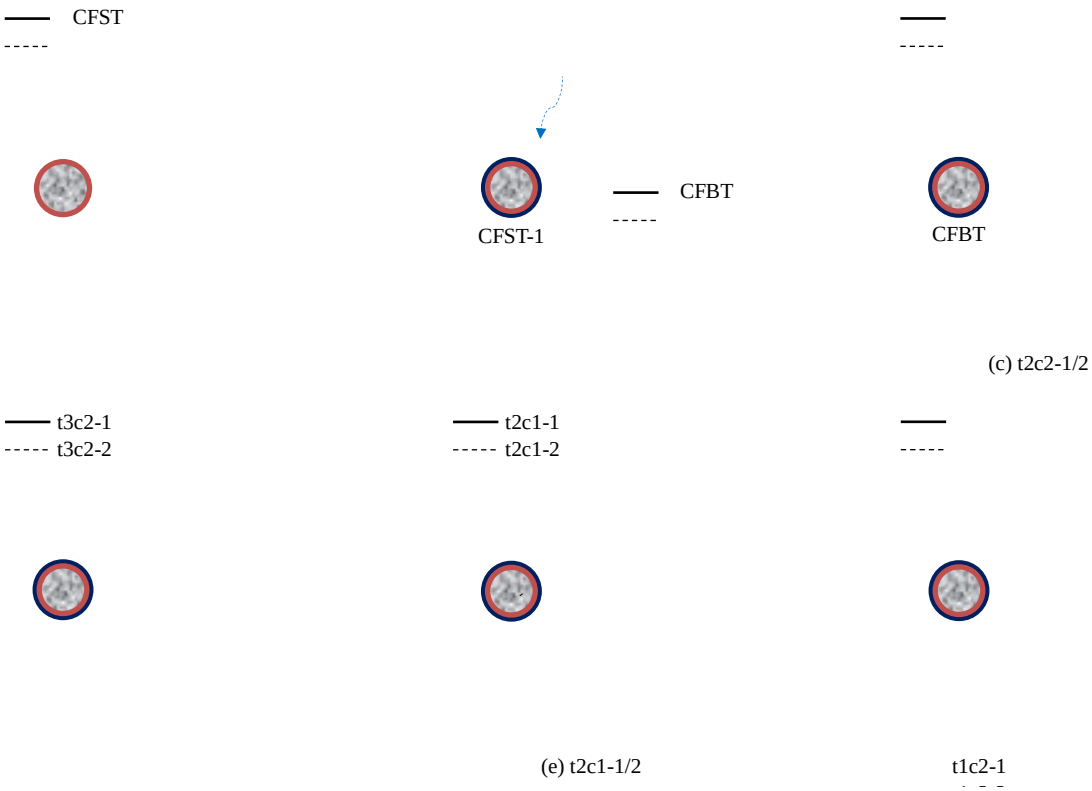

Fig. 10 Axial load (N) versus deformation (Δ) relationships of CFST and CFBT short columns

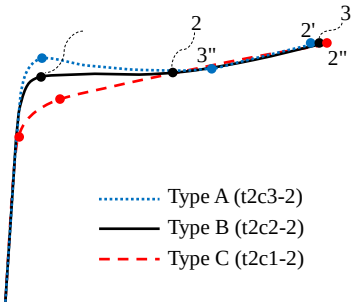

Fig. 11 Typical axial load (N) versus axial strain (ε) curves for CFBT short columns

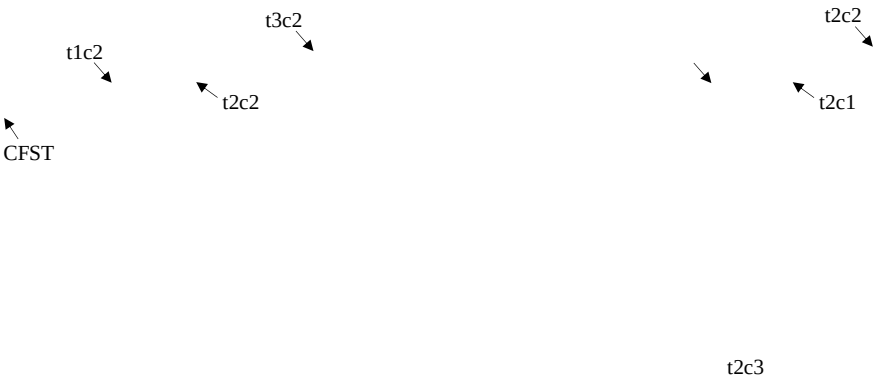

Fig. 12 Effects of test parameters on axial strength of CFBT specimens

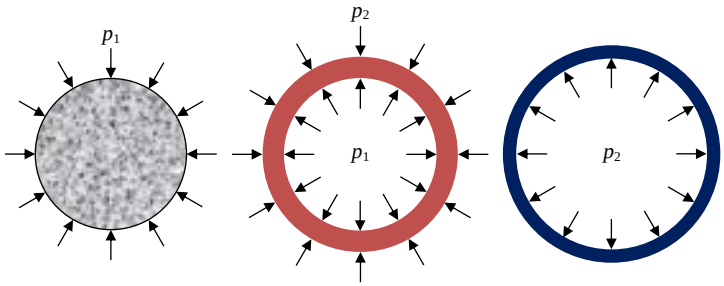

(a) Concrete core (b) Carbon steel tube layer (c) Stainless steel tube layer

Fig. 13 Schematic of composite actions between different components of the CFBT section

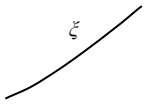

Fig. 14 Strength index (*SI*) versus confinement factor (ξ) relationship

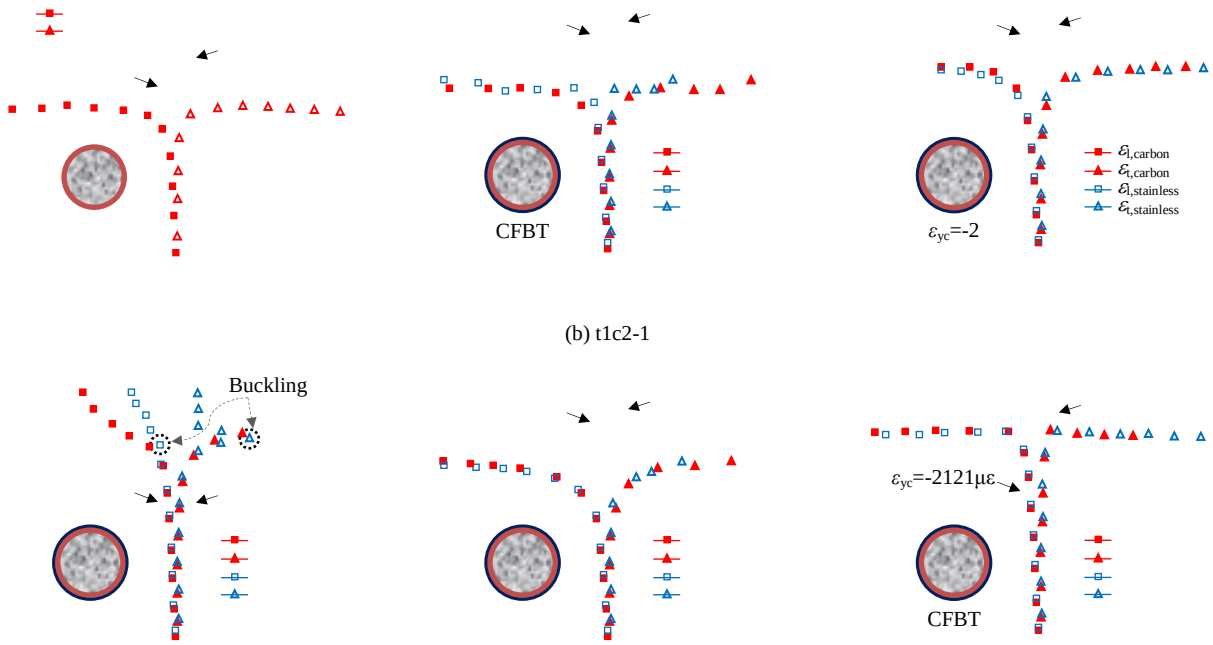

Fig. 15 Axial load (N) versus steel strain (ε_s) relationships of CFST and CFBT short columns

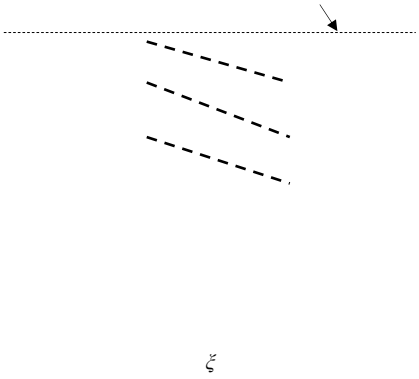

Fig. 16 Comparison of axial strengths between predicted values (N_{uc}) and experimental results (N_{ue})